The genetic architecture of floral trait divergence between hummingbird- and self-pollinated monkeyflower (*Mimulus*) species

Hongfei Chen[1,5], Colette S. Berg[2], Matthew Samuli[2], V. Alex Sotola[3,4], Andrea L. Sweigart[3], Yao-Wu Yuan[1*], Lila Fishman[2*]

[1] Department of Ecology and Evolutionary Biology, University of Connecticut, Storrs, CT 06269 USA

[2] Division of Biological Sciences, University of Montana, Missoula MT 59812 USA

[3] Department of Genetics, University of Georgia, Athens, GA 30602, USA.

[4]Current address: Biology Department, State University of New York at Oneonta, Oneonta, NY 13820 USA

[5] Current address: Department of Ecology and Evolutionary Biology, Yale University, New Haven, CT 06520 USA

[*]For correspondence

SUMMARY

1) Pollination syndromes are a key component of flowering plant diversification, prompting questions about the architecture of single traits and genetic coordination among traits. Here, we investigate the genomic basis of extreme floral divergence between naturally hybridizing monkeyflowers *Mimulus parishii* (self-pollinated) and *M. cardinalis* (hummingbird-pollinated).

(2) We mapped quantitative trait loci (QTLs) for 18 (nine fully shared) pigment, pollinator reward and handling, dimensional, and flowering time traits in two F_2 hybrid growouts and recombinant inbred lines. We independently generated nearly isogenic lines (NILs) to dissect QTLs for two dimensional traits, pistil length and corolla size.

(3) Our multi-population approach revealed a highly polygenic basis (n = 190 QTLs total) for pollination syndrome divergence. For the set of nine fully shared traits, 39% (55/140) were unique to a single population, but we also identified several QTL hotspots within and across trait categories. The complementary NIL approach refined two pistil length QTLs but selected a corolla size QTL resistant to genetic dissection.

(4) Divergence between hummingbird- and self-pollinated sister species has a highly polygenic and largely uncoordinated genetic architecture. Our results extend understanding of speciation in a classic floral radiation and provide a robust framework for further molecular dissection and ecological genomics.

KEYWORDS – genetic architecture, QTL mapping, modularity, pollination syndrome, polygenic trait

Introduction

Across flowering plants, distantly related taxa often show similarities in a suite of floral phenotypes that can be recognized as pollination syndromes (Fenster *et al.*, 2004; Dellinger, 2020), while switches between pollination syndromes are common even among closely related species. For example, the evolution from bee- to hummingbird-pollination, which is characterized by red color, copious nectar, and stigma and anthers exerted beyond a large bill-accommodating corolla, has happened more than 10 times independently in *Penstemon* alone (Wilson *et al.*, 2007; Wessinger & Hileman, 2016). Similarly, routine self-pollination, which is associated with inconspicuous coloration, reduced nectar rewards, and reduced anther-stigma separation (Sicard & Lenhard, 2011), has evolved countless times within animal-pollinated lineages (Stebbins, 1970; Barrett, 2002; Goodwillie *et al.*, 2005). Both convergence and divergence in pollination syndromes requires the correlated evolution of multiple traits to maintain floral phenotypic integration and reproductive fitness throughout the entire evolutionary path. Natural selection on floral traits may be strong enough to restrict successful plants to a few discrete adaptive peaks (Bleiweiss, 2001), building distinct syndromes from independent and continuous genetic variation. However, fundamental genetic correlations (pleiotropy) among traits (Troth *et al.*, 2018) may facilitate coordinated evolution during pollination syndrome divergence (Smith, 2016; Wessinger & Hileman, 2016). Finally, genome architectures (e.g. inversions) that suppress recombination in heterozygotes can package genes for functionally distinct traits into adaptive supergenes (Lowry & Willis, 2010; Hermann *et al.*, 2013; Edwards *et al.*, 2021; Liang *et al.*, 2023). These three (non-exclusive) explanations for multi-trait syndromes in extant taxa imply very different barriers to traversing the phenotypic landscape between alternative peaks. Thus, understanding the genetic mechanisms that underlie suites of floral traits illuminates their individual evolutionary histories but also reveals the roles of genomic architecture as flowers evolve coordinately from one multi-phenotypic optimum to another.

Over the past three decades, quantitative trait locus (QTL) mapping has revealed the genetic architecture of pollination syndrome divergence between numerous closely-related pairs of plant species, including three sections of *Mimulus* monkeyflowers (Bradshaw *et al.*, 1998; Fishman *et al.*, 2002, 2013, 2015; Stankowski *et al.*, 2023), *Petunia* (Stuurman *et al.*, 2004), *Ipomoea* (Rifkin *et al.*, 2021; Liao *et al.*, 2021) and many others. Across angiosperm diversity from monocots to diverse eudicots, these genome-wide approaches reveal two broad patterns. First, divergence in pollinator-attraction and reward traits such as flower color, scent, or nectar volume is often controlled by few loci, each of moderate to large effect, whereas divergence in dimensional traits (corolla or reproductive organ size

67 and shape) often involves more loci, each of small effect. This pattern may in part reflect focus on
68 attraction/reward in stark transitions among distinct animal pollination syndromes and a primary focus on
69 floral dimensions in shifts to selfing. However, it may also reflect consistent differences in the underlying
70 genetic variation (e.g., standing variation vs. new mutations) and selective landscape (e.g. rugged vs.
71 smooth) for different traits. Second, co-localization of QTLs for at least some floral traits suggests floral
72 integration through pleiotropy and/or the adaptive evolution of supergene architecture to facilitate trait
73 packaging in the face of gene flow (Yeaman & Whitlock, 2011). Understanding both the build-up and the
74 breakdown of trait correlations to generate complex floral strategies requires a locus- and gene-scale
75 understanding of the genomic bases of pollination syndromes.

76 Although QTL mapping has robustly advanced understanding of the genetic architecture of divergence
77 in multi-factorial trait syndromes, connecting their effects to the underlying genes remains a challenge.
78 First, especially when traits are polygenic and the underlying loci have small effects, scans of single
79 experimental hybrid mapping populations capture the overall architecture of genetic variation, but not
80 individual loci and their effects. Thus, replication of mapping experiments tests QTL robustness to
81 environmental variation and increases confidence in shared QTLs. Second, even major QTLs often
82 contain 10s to 100s of genes, confounding pleiotropy and linkage as causes of genetic correlation and
83 QTL coincidence. Similarly, fine-scale identification of causal variants benefits from isolation from
84 segregating background effects. Construction of near-isogenic lines (NILs) allows both detection and
85 isolation, as in the identification of major flower color and scent loci in *Petunia* (e.g. (Klahre *et al.*, 2011;
86 Berardi *et al.*, 2021) and *Mimulus* (Bradshaw & Schemske, 2003; Yuan *et al.*, 2013b; Byers *et al.*, 2014;
87 Yuan *et al.*, 2016; Liang *et al.*, 2023). However, because NIL construction generally involves strong
88 selection for resemblance to the introgressing parent for a focal trait combined with opposing selection
89 on other traits, it may not capture the evolutionary contributions of more complex genetic architectures
90 to trait (co-)variation. Thus, a combination of replicated genome-wide QTL characterization plus targeted
91 NIL construction is a powerful approach to understand both the genome-wide architecture and gene-
92 scale causes of divergence in complex pollination syndromes.

93 Here, we employ an integrated approach to characterize the genetic architecture of pollination
94 syndrome divergence and the detailed genetics of key traits between closely related monkeyflowers
95 *Mimulus cardinalis* and *M. parishii* (Phyrmaceae, section *Erythranthe*). These taxa, which are
96 hummingbird-pollinated and self-pollinated, respectively (Fig. 1), are the most florally divergent
97 members of a recent adaptive radiation (Nelson *et al.*, 2021b). Nevertheless, they hybridize in areas of

range overlap, producing genomic signatures of recent introgression (Nelson *et al.*, 2021b). Along with bee-pollinated *M. lewisii*, which likely resembles the common ancestor of all three taxa, these closely related species are a model system for understanding the genetics of floral divergence and speciation (Yuan, 2019). Work in this system has provided key insights into the evolution and molecular biology of divergent pollination syndromes and their roles in local adaptation and speciation (Hiesey *et al.*, 1971; Bradshaw *et al.*, 1995; Schemske & Bradshaw, 1999; Ramsey *et al.*, 2003; Fishman *et al.*, 2013; Yuan *et al.*, 2013b, 2014; Stathos & Fishman, 2014; Fishman *et al.*, 2015; Yuan *et al.*, 2016; Peng *et al.*, 2017; Nelson *et al.*, 2021b,a; Liang *et al.*, 2023). New resources, including chromosome-scale reference genomes (www.Mimubase.org), dense linkage maps (Sotola *et al.*, 2023), and stable transformation protocols (Yuan, 2019), now enable genome-wide mapping, gene-scale dissection, and molecular characterization of the loci underlying *Erythranthe* floral diversity. Importantly, because *Mimulus parishii* x *M. cardinalis* hybrids segregate more freely than other crosses in the group (Fishman *et al.*, 2013, 2015; Sotola *et al.*, 2023), they were key to the recent genetic and molecular dissection of a novel speciation supergene (Liang *et al.*, 2023). With the current study, we take a major step toward a similarly detailed understanding of the full suite of floral traits contributing to pollination syndrome divergence.

To robustly characterize the genetic architecture of extreme floral divergence, we examine patterns of floral trait (co)inheritance and map QTLs in one extensively phenotyped focal F_2 population, then map QTLs for a subset of traits in independent F_2 and RIL growouts. We assess QTL coincidence within and across trait categories and ask whether genomic architectures and individual loci are shared with previous *M. parishii* x *M. lewisii* (Fishman *et al.*, 2015) and *M. lewisii* x *M. cardinalis* hybrids (Bradshaw *et al.*, 1995, 1998; Fishman *et al.*, 2013). We then construct and characterize NILs for two key dimensional traits, flower size and pistil length, which are among the most challenging traits for genetic analysis due to their generally polygenic nature. In addition to illuminating the genetics of flower size evolution, these NILs provide inspiring proof of concept (and sound some useful cautionary notes) on the dissection of dimensional QTLs. Our multi-trait and multi-generation approaches provides a broad and deep characterization of the genetics of floral divergence and opens paths toward understanding both its molecular bases and effects on patterns of mating and introgression in wild populations.

Materials and Methods

Study system, mapping populations, and phenotyping

127 Hummingbird-pollinated *M. cardinalis* (Phrymaceae) is a perennial herb of low-elevation seeps and river
128 banks from northern Baja California to southern Oregon (Angert & Schemske, 2005; Angert, 2009). It has
129 red flowers with long tubular corolla, copious nectar, and exserted stigma and anthers (Fig. 1a). *M.*
130 *parishii* is an annual self-pollinating herb generally found along ephemeral streams in southern California.
131 *M. parishii* has small pale pink flowers, little stigma–anther separation, and no nectar (Fig. 1a). All hybrids
132 in this study were generated from two highly inbred parental lines: Sierran CE10 for *M. cardinalis* (Yuan
133 *et al.*, 2013b) and PAR for *M. parishii* (Fishman *et al.*, 2015; Nelson *et al.*, 2021b; Liang *et al.*, 2023). F_1
134 hybrids were generated with PAR as the seed parent and selfed to generate F_2 seeds, while recombinant
135 inbred lines (RILs) were generated by single-seed-descent from F_2 individuals through 3-6 generations of
136 self-fertilization (Sotola *et al.*, 2023). F_2 hybrids were grown in two separate greenhouse common
137 gardens at the University of Connecticut (UC_F_2) and the University of Montana (UM_F_2), and the RILs
138 were grown at the University of Georgia (UGA), as detailed in Supplementary Methods S1.

139 In the UC_F_2 growout, we measured three pigment, two pollinator reward/handling and nine
140 dimensional floral traits, plus flowering time, on F_2s (n = 253) plus parental lines and F_1 hybrids (n =8
141 each) (Fig. 1). We scanned the ventral petal of each flower to quantify petal lobe anthocyanin (PLA) and
142 carotenoid (PLC) pigment intensity. The proportion of red (R), green (G), and blue (B) pixels in a square
143 area of the same size of the adaxial surface of the petal were estimated from scanned images using
144 Image J (http://rsbweb.nih.gov/ij/) and the relative petal lobe anthocyanin and carotenoid
145 concentrations estimated by [(R + B)/2] − G and [(R + G)/2] – B, respectively. Nectar guide anthocyanin
146 (NGA) and nectar guide trichome length (NGT), were visually scored in F_1 and F_2 hybrids on semi-
147 quantitative scales defined by the parental extremes (CARD = 9 and 7, respectively, PAR = 1 for both).
148 Nectar volume (NEV) was measured for two flowers per individual on their first day of opening, using a
149 pipette accurate to 1.5μL. To reduce environmental effects, nectar was measured at 4:00 PM-7:00 PM
150 after watering at 12:00-1:00PM each day. Floral dimensions (Fig. 1c) were measured on one of the
151 second pair of open flowers using a digital caliper, and stigma-anther distance calculated as pistil length
152 – stamen length. We then calculated phenotypic means for all four genotypic classes, mid-parent
153 values, environmental standard deviations, and broad-sense heritability for each trait following (Fishman
154 *et al.*, 2002). F_2 distributions were tested for normality with a Shapiro–Wilk test implemented in R v.
155 3.6.0. Because some traits were non-normally distributed, we calculated pairwise Spearman's correlation
156 coefficients (r) for phenotypic correlations using the *psych::corr.test* function in R v. 3.6.0. ; we calculated
157 genotypic correlations following (Fishman *et al.*, 2002).

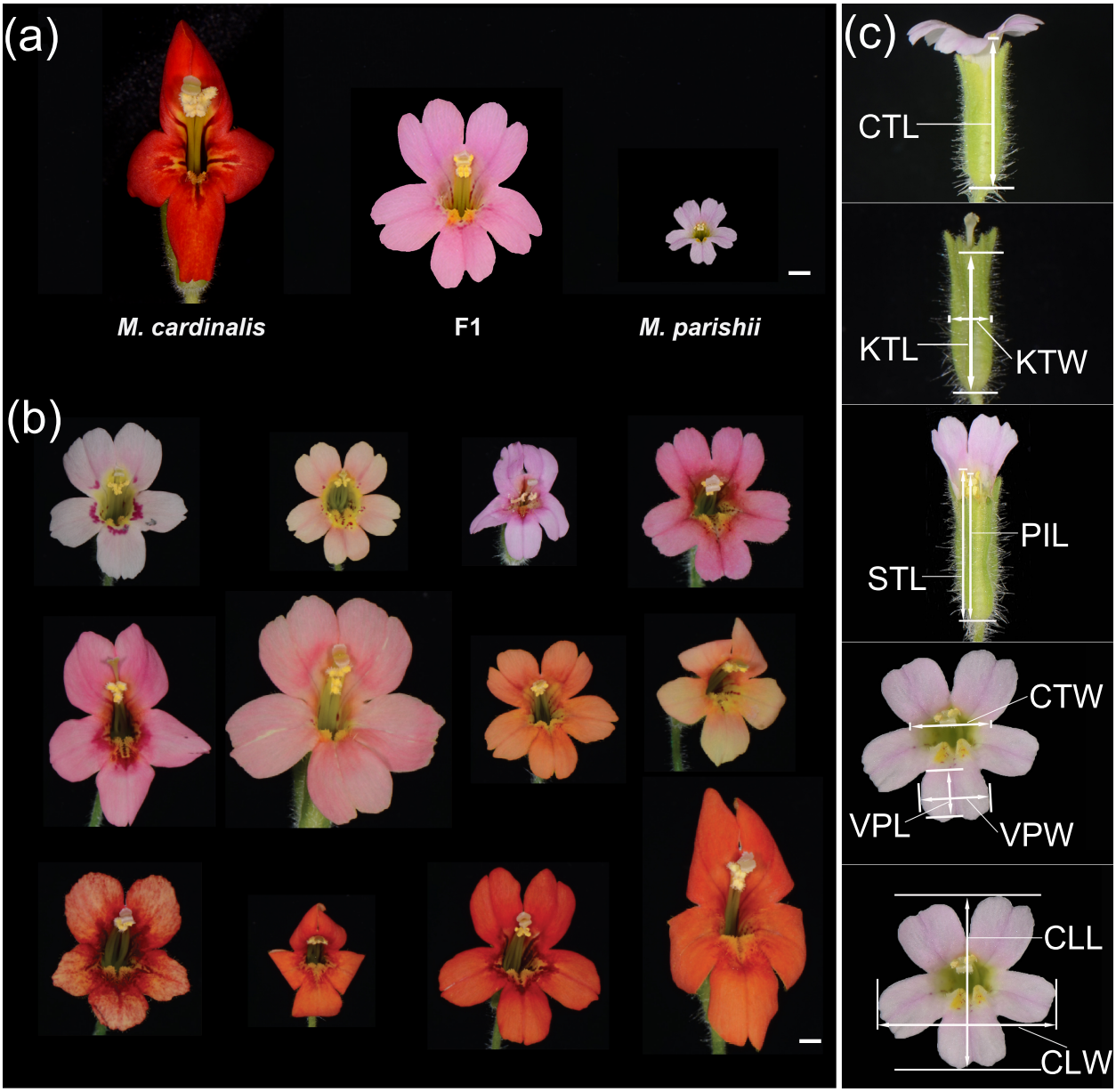

158

Fig. 1 Floral phenotypes. (a) The parental line *M. cardinalis* CE10, *M. parishii* PAR, and their F_1 hybrid. (b) Representative F_2 progeny. (c) The floral dimensions traits measured in this study, shown on *M. parishii*. CTL: corolla tube length; KTL: calyx tube length; KTW: calyx tube width; STL: stamen length; PIL: pistil length; CTW: corolla tube width; VPL: ventral petal length; VPW: ventral petal width; CLL: corolla limb length; CLW: corolla limb width. Scale bars, 3 mm.

159 Overlapping subsets of key floral traits were measured using parallel methods in the UM_F_2 (n = 278)
160 and UGA_RIL growouts (n = 145) (Supplementary Methods S2). Traits with a shared abbreviation
161 represent the same floral dimension, with the exception of pistil length (PIL) and stigma-anther
162 separation (SAS), which included the stigma lobes in the UC_F_2 and UGA_RILs (Fig. 1c) but not the
163 UM_F_2s. In the UM_F_2 growout, we characterized an additional pollinator handling trait associated with

164 pollination syndrome divergence in *Mimulus*, touch-sensitive stigma closure (Friedman *et al.*, 2017). The
165 bilobed stigmas of *M. cardinalis* close rapidly (<5s; like a tiny venus flytrap) when touched, while *M.*
166 *parishii* stigmas are insensitive and/or non-closing (Fishman *et al.*, 2024). Prior to the other floral
167 measurements, a single tester touched each stigma head-on with a pencil eraser to mimic pollinator
168 contact and scored stigma closure speed on a 4-point scale (0 = no closure = PAR-like, 3 = fast closure =
169 CE10-like, ~3 seconds, 1 and 2 = slower [>6 seconds] and faster [3-6 seconds] intermediates,
170 respectively).

171 Genetic context and QTL mapping

172 We constructed a joint linkage map of the two F_2 populations and a separate map of the RILs using
173 windowed genotypes from ddRAD sequences aligned to the CE10 *M. cardinalis* reference genome
174 (Sotola *et al.*, 2023). The dense F_2 and RIL linkage maps are generally highly collinear with each other
175 and the physical genome assemblies (www.Mimubase.org). However, an *M. cardinalis*-specific reciprocal
176 translocation causes complex linkage, excess heterozygosity, and underdominant hybrid sterility on Chr6
177 and Chr7 (LG6&7), while a gametophytic Dobzhansky-Muller incompatibility involving Chr4 (~7-8 Mb)
178 and Chr8 (~12-40 Mb) eliminates three genotypic classes in F_2 and later hybrids (Sotola *et al.*, 2023).

179 We conducted QTL mapping in QTL Cartographer (Wang *et al.*, 2005) in parallel on the three
180 populations using composite interval mapping (model 6, with forward-backward regression to choose 10
181 cofactors, window size 10 cM). LOD significance thresholds for QTL detection for each trait were set with
182 1000 permutations. Due to substantial retained heterozygosity in the RILs (Sotola *et al.*, 2023), we used
183 F_2 rather than RIL population settings to allow full estimation of QTL effects using all individuals. To
184 evaluate QTL coincidence across populations and traits, as well as define physical bounds, we defined a
185 1.5 LOD-drop confidence interval (CI) around each peak. For the two F_2 populations, which share a
186 linkage map, overlap was directly determined. For comparing F_2s and RILs, we translated QTL peaks and
187 intervals to the physical positions of boundary markers. We assigned QTL numbers within traits across
188 populations on the basis of CI overlap (Table S1). For floral dimensions, where there are apparent QTL
189 hotspots that span populations and traits, we further attempted to bin QTLs into a smaller number of
190 "size QTLs". However, although there are some regions of tight coincidence (e.g. at ~ 40cM on Chr2),
191 sets of serially overlapping QTLs (or one broad one) often defined whole chromosome arms and are
192 unlikely to represent shared underlying loci. Therefore, we do not formally designate shared bins here.

193

194 Construction and characterization of nearly isogenic lines (NILs)

195 NILs were constructed via phenotypic selection prior to QTL mapping, and thus provide an independent
196 approach to dissecting the genetics of dimensional traits. To construct pistil length (PIL) NILs in the *M.*
197 *parishii* genetic background, we chose an F_2 individual with overall similarity to *M. parishii* in both floral
198 and vegetative traits, but with conspicuously longer pistil, for serial backcrossing (with NIL as pollen
199 donor) to *M. parishii.* From each backcross growout of ~95 plants, we selected one individual that
200 closely resembled *M. parishii* but with longer pistil for the next round. Genotyping a BC_3S_1 population
201 revealed two chromosome fragments (Chr 4: 0-4.1 Mb; Chr 6: 42-52 Mb) introgressed from *M. cardinalis*
202 co-segregating with pistil length. Selfing a BC_3S_1 individual that is heterozygous for both fragments
203 generated nine genotypes across the two loci, which also allowed us to decompose the BC_3 NIL into two
204 NILs. A similar crossing approach was used to generate a corolla limb length (CLL) NIL representing
205 flower size (Supplementary Methods S3).

206 **Table 1. Floral trait variation (means +/- SE for *M. cardinalis* (CE10), *M. parishii* (PAR), and their F_1 and F_2 hybrids**
207 **in UC_F_2 growout.** Broad-sense heritability (H^2) was calculated following Fishman *et al.* (2002). Traits marked **
208 were also measured in both UM_F_2 and RIL mapping populations, while nectar volume (NEV; *) was also
209 characterized in RILs. See Fig. S1 for trait distributions in all populations.

210

Trait	*M. cardinalis* CE10 (n=8)	*M. parishii* PAR (n=8)	F_1 hybrid (n=8)	F_2 hybrids (n=253)	H^2
Pigment					
Petal lobe carotenoid (PLC)**	99.38 ± 0.44	2.29 ± 0.50	13.89 ± 0.48	48.01 ± 2.12	1.00
Petal lobe anthocyanin (PLA)**	74.39 ± 1.11	21.46 ± 1.93	64.15 ± 1.02	52.38 ± 1.23	0.96
Nectar guide anthocyanin (NGA)	9	1	5	5.20 ± 0.12	NA
Pollinator reward/handling					
Nectar volume (NEV)*	45.95 ± 3.83	0 ± 0	3.28 ± 0.17	5.30± 0.29	-0.35
Nectar guide trichome (NGT)	7	1	4	4.40 ± 0.10	NA
Dimension					
Corolla limb length (CLL)	36.45 ± 0.69	8.18 ± 0.09	19.97 ± 0.49	20.21 ± 0.26	0.89
Corolla limb width (CLW) **	20.23 ± 1.62	8.94 ± 0.09	18.61 ± 0.43	18.30 ± 0.22	0.49
Ventral petal width (VPW)	12.46 ± 0.39	3.28 ± 0.07	7.27 ± 0.12	7.52 ± 0.09	0.82
Ventral petal length (VPL)	10.43 ± 0.21	2.77 ± 0.06	5.51 ± 0.10	6.11 ± 0.07	0.91
Corolla tube width (CTW)**	8.29 ± 0.27	4.43 ± 0.27	7.69 ± 0.15	7.26 ± 0.08	0.84
Calyx tube length (KTL)	22.30 ± 0.17	9.82 ± 0.28	16.17 ± 0.29	16.90 ± 0.14	0.90
Calyx tube width (KTW)	7.68 ± 0.13	2.98 ± 0.08	5.06 ± 0.08	5.34 ± 0.06	0.91
Corolla tube length (CTL)**	32.85 ± 0.35	11.74 ± 0.31	21.68 ± 0.23	22.46 ± 0.20	0.93
Pistil length (PIL)**	45.88 ± 0.43	11.76 ± 0.21	25.89 ± 0.29	27.20 ± 0.28	0.96
Stamen length (STL)**	42.93 ± 0.28	13.31 ± 0.47	24.91 ± 0.27	25.30 ± 0.24	0.94
Stigma-anther separation (SAS)**	2.95 ± 0.28	-1.55 ± 0.34	0.99 ±0.16	1.90 ± 0.09	0.71
Flowering time (FLT)**	79.38 ± 0.84	53.5 ± 1.07	55.13 ± 0.30	66.68 ± 0.51	0.94

211
212

Results

Phenotypic divergence, distributions, and correlations in F_2 hybrids

In the focal UC_F_2 growout, the CE10 *M. cardinalis* and PAR *M. parishii* parental lines were highly differentiated for all traits, with F_1 and F_2 means always intermediate (Table 1). Floral dimensions were normally distributed in F_2s, but petal carotenoid values (PLC) were bimodally distributed while petal lobe anthocyanins (PLA) were skewed toward CE10 and nectar volume (NEV) toward PAR (Fig. S1). NEV had negative H^2 estimates due to its extreme skew toward low values, but other quantitative traits showed high broad-sense heritability ($H^2 > 0.49$). The UM_F_2 and RILs showed similar distributions for each shared trait, but nectar volume was much higher in the RILs (Fig. S1). In the UC_F_2s, all floral dimensions other than stigma-anther separation (SAS) were positively correlated both phenotypically (r_P) and genetically (r_G) (Fig. 2). Stigma-anther separation (SAS) was most highly correlated with pistil length (r_G = 0.57), less with the other length metrics (r_G = 0.25 - 0.31), and uncorrelated with width metrics. Floral dimensional traits were only moderately correlated with flowering time (FLT) but flower length traits (KTL, CTL, STL, PIL) were correlated with nectar volume (r_P= 0.58-0.70, r_G not calculable for NEV due to negative H^2) and petal lobe carotenoids were strongly correlated with pistil length and stamen length (both $r_G > 0.6$).

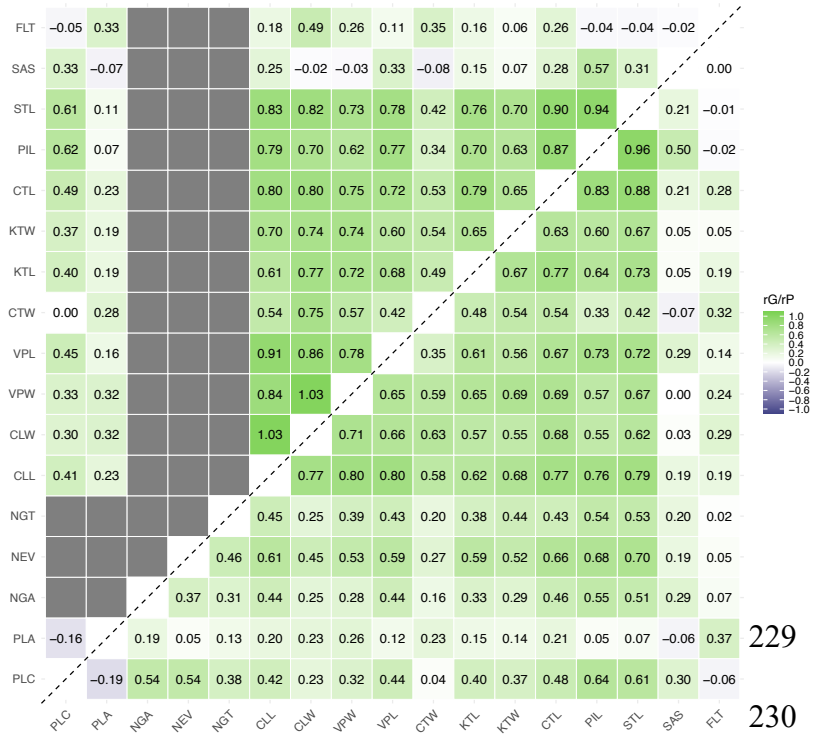

Fig. 2. Phenotypic (rP; below diagonal) and genetic (rG; above diagonal) correlations among traits in the *M. parishii* x *M. cardinalis* UC_F_2. PLC: petal lobe carotenoid; PLA: petal lobe anthocyanin; NGA: nectar guide anthocyanin; NEV: nectar volume; NGT: nectar guide trichome; CLL: corolla limb length; CLW: corolla limb width; VPW: ventral petal width; VPL: ventral petal length; CTW: corolla tube width; KTW: calyx tube width; KTL: calyx tube length; CTL: corolla tube length; STL: stamen length; PIL: pistil length; SAS: stigma-anther separation; FLT: flowering time.

231 **QTL mapping – genetic architecture across traits and populations**

232 We identified 190 floral QTLs, which define 144 QTL locations if collapsed (within traits) across the three
233 mapping populations (Fig. 3, Table S1).

234 *Pigment traits* -- As expected from previous work, petal lobe carotenoids (PLC) were primarily affected
235 by a fully shared *M. cardinalis*-recessive major QTL on LG4 (coincident with YUP; PLC4.1 in Table S1). We
236 also detected two additional smaller carotenoid loci in the F_2s, and two more in the RILs. For petal lobe
237 anthocyanins (PLA), four loci were detected: PLA4.1 was detected in all three growouts and coincident
238 with the *YUP-SOLAR-PELAN* supergene, PLA4.2 and PLA3 were found in both F_2s but not the RILs and
239 PLA6&7 was found in the RILs and UC_F_2. Nectar guide anthocyanins (NGA) were under the control of
240 two major loci, NGA3 (r^2 = 0.21) and NGA4 (r^2 = 0.31), and two additional small QTLs. Except for
241 PLA6&7, at which *M. parishii* alleles increased anthocyanins in both UC_F_2 and RILs, all pigment QTLs
242 had effects consistent with the direction of parental divergence.

243 *Reward and handling traits* – We detected four nectar volume QTLs in the UC_F_2 and two completely
244 non-overlapping ones in the RILs. RIL QTLs NEV5 and NEV8 had absolutely ~4x larger effects than the
245 largest F_2 one (NEV6&7; r^2 = 0.20), which explained only ~1/7 of the parental difference in NEV. The four
246 largest NEV QTLs (RIL pair, plus NEV2 and NEV6&7) were each coincident with dense clusters of floral
247 dimension QTLs (see below). Nectar guide trichomes (NGT) and touch-sensitive stigma closure speed
248 (SCS) QTLs, which scored on semi-quantitative scales, had relatively low explanatory power in the
249 segregating F_2 populations (all r^2: 0.04-0.11). However, QTLs for these traits explained from 20% (each of
250 the two *M. parishii*-recessive stigma closure QTLs: SCS5 and SCS6&7) to 40% of the parental difference
251 (additive NGT8). Thus, they provide key targets for understanding the genetic underpinning of these
252 important but understudied non-pigment components of floral syndrome evolution.

253 *Dimensional traits* – In the UC_F_2, floral size was highly polygenic; excluding the composite trait of
254 stigma-anther separation, we detected a total of 71 dimensional QTLs. QTL sizes were correspondingly
255 small, with the leading QTL for each trait explaining 11% (CLL, CTL, KTW) to ~20% (VPL, VPW) of the F_2
256 variance. All size QTLs in this F_2 population moved trait values in the direction expected by the parental
257 difference; however, 2 of the 6 QTLs for stigma-anther separation, which depends on differences in the
258 relative length of highly correlated male and female reproductive organs, had opposite effects from
259 expectation; this is consistent with the transgressive segregation for this trait in the F_2s (Fig. S1). QTLs
260 for different size traits were often coincident; for example, the first 5 Mb of Chr2 and Chr8 each housed

261 overlapping UC_F_2 QTLs for 8 of the 11 floral dimensions. This co-incidence may not represent
262 pleiotropic effects of single variants, as *Mimulus* chromosome ends are gene-dense and highly
263 recombining (Nelson *et al.*, 2021a), but these regions are promising targets for dissection of multiple
264 traits.

265 For the shared six core dimensional traits, we mapped 43, 39 and 29 QTLs in the UC_F2, UM_F2 and
266 RILs, respectively, and ~1/3 (35/111) were shared across two or more populations. Repeatability across
267 experiments suggests that even the smallest shared QTLs reflect robust association between a given
268 genomic region and dimensional variation, but it is also clear that each mapping population adds novel
269 (small) loci for these polygenic traits. Overall, >95% (139/145) of dimensional QTL allele substitutions
270 moved hybrid trait values in the direction expected from the parental difference. Four of the exceptions
271 were stigma-anther separation QTLs, and the other two were corolla tube length and width QTLs
272 (CTL5.1 and CTW5.1) at a shared position in the UM_F_2. Although QTLs within this trait group are not
273 independent (Fig. 3), this overwhelming consistency suggests directional natural selection in one or both
274 parental lineages (Orr, 1998).

275 Flowering time departed from the pattern of repeatability. FLT4.1 (all three mapping populations) and
276 FLT8.1 (UC_F_2 and RILs) were shared, but the other 7 QTLs were each found in only a single population.
277 Flowering time QTLs are not particularly small (all $r^2 > 0.07$, $2a > 6$ days), so this likely reflects true
278 genotype x environment interactions for phenology. FLT4.1, at which *M. parishii* alleles confer much
279 earlier flowering ($2a$ = 7.8 to 18.6 days), shares a 0.5-1Mb region on Chr4 with a partially overlapping set
280 of 13 floral-size QTLs (across all populations). This QTL co-localization may indicate linkage among
281 functionally distinct genes in a gene-dense chromosomal region, but it could reflect a flowering time
282 locus that pleiotropically mediates tradeoffs between speed and size (i.e., fast flowering = small flowers),
283 as in *M. guttatus* (Troth *et al.*, 2018).

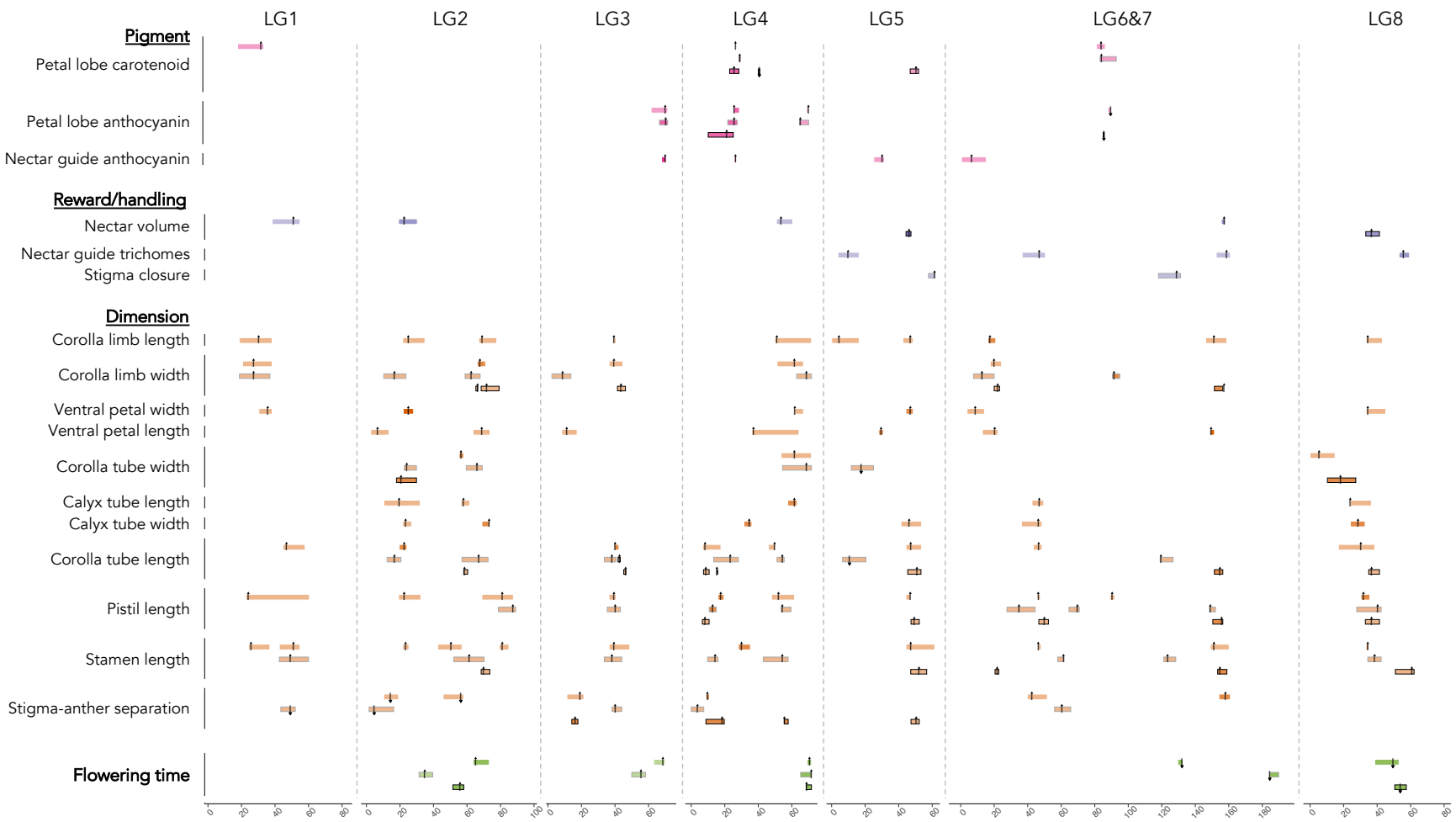

284

Fig. 3. Quantitative trait loci (QTLs) for floral traits associated with pollination syndrome divergence between selfer *Mimulus parishii* and hummingbird pollinated *M. cardinalis*, as detected in three mapping populations. Bars show QTL 1.5 LOD drop confidence intervals and arrows indicate QTL peak position (up = QTL effect is in direction expected from parental divergence, down = opposite). The UCF2 QTL bars (all traits other than stigma closure) are unbordered, UM_F2 QTL bars are bordered in gray, and RIL QTL bars are bordered in black. The x-axis is position in centiMorgans (cM) on each of the seven linkage groups, which correspond to eight chromosomes due to a reciprocal translocation between Chr 6 and Chr 7 in *M. cardinalis* vs. *M. parishii*.

285 Dissection of two floral dimension QTLs with NILs

286 The long-pistil (PIL) and flower size (CLL) NILs isolated *M. cardinalis* alleles in the *M. parishii* background
287 using repeated rounds of backcrossing and selfing with phenotypic selection (Supplemental Methods
288 S3). The long-pistil NIL contained two unlinked regions introgressed from *M. cardinalis*, corresponding
289 to QTLs *PIL4.1* (0-4.1 Mb on Chr4) and *PIL6&7.2* (42.85 Mb-51.76 Mb on Chr6; Fig. 4b). In a BC_3S_1
290 population segregating for all genotypic combinations at these two loci, both QTLs exhibited primarily
291 additive effects on pistil length, consistent with the estimated QTL effects. The two NIL-isolated QTLs
292 both had absolute effects smaller than in the F_2 population but maintained their relative sizes: *PIL4.1* (2*a*
293 = 5.68mm in F2s, 3mm in NIL) vs. *PIL6&7.2* (2*a* = 4.24mm in F2s, 1mm in NIL). There was no evidence of
294 an epistatic interaction between these two loci, as the double NIL was 4mm larger than *M. parishii* (Table
295 S2). The CE10-homozygous *PIL4.1* NIL also increased stamen and corolla tube lengths, but not our
296 measure of overall flower size (CLL), relative to *M. parishii* (Table 2). In contrast, the *PIL6&7.2* NIL had
297 little effect on stamen or corolla tube length (Table S2), suggesting that *PIL6&7.2* contains a gene that
298 specifically regulates pistil length.

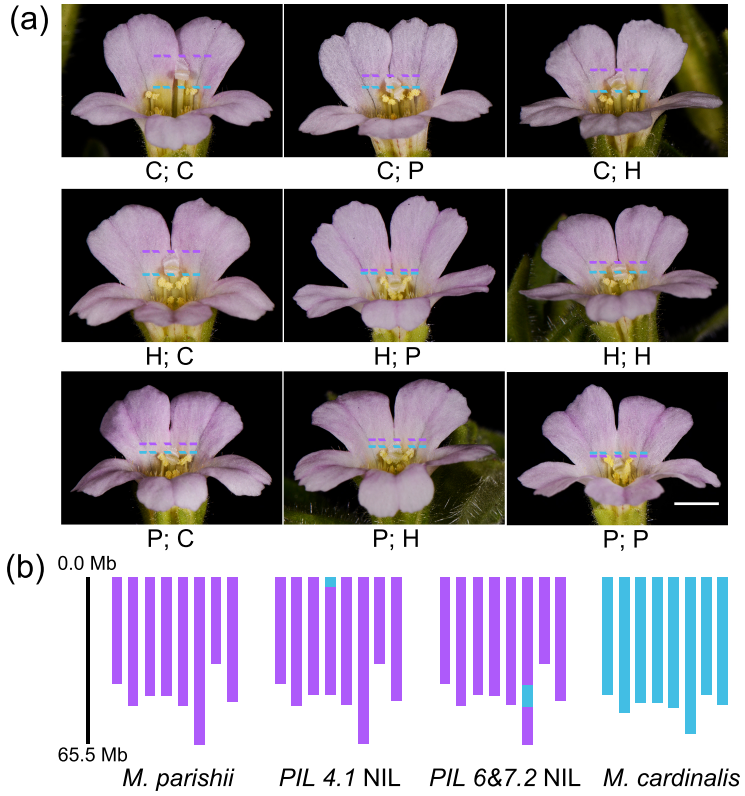

Fig. 4. Pistil NILs. (a) Phenotypes of 9 genotypic combinations of the *PIL4.1* and *PIL6&7.2* loci. Genotypic designations: C, homozygous for *M. cardinalis*; H, heterozygous; P, homozygous for *M. parishii*. Under each image, the *PIL4.1*genotype is followed by the *PIL6&7.2* genotype. The colored dashed lines indicate the positions of the stigmas and long stamens, respectively. Scale bar, 3 mm. (b) Graphical genotypes of the *PIL4.1* NIL and the *PIL6&7.2* NIL. The colored bars represent the 8 chromosomes

300

After selfing and phenotypic selection (Supplemental Methods S3), the final BC_3S_1 NIL for corolla limb length (CLL) captured a large region including *CLL6&7.2* (Fig. 5). This NIL was heterozygous across much of Chr6 (43.54Mb-60.3Mb) and Chr7 (0-29.34Mb), but *M. cardinalis* homozygous near the LG6&7 translocation breakpoint (60.32Mb-61.12Mb on Chr6; 29.34Mb-29.82Mb on Chr7). Unlike the more tightly localized *PIL6&7.2* introgression (which it includes in heterozygous state), the *CLL6&7.2* NIL has increased pistil, stamen, and corolla tube length, as well as greater CLL, relative to *M. parishii* (Fig. 5a, Table S3). Because the *CLL6&7.2* NIL includes a recombination-suppressed translocation breakpoint associated with underdominant pollen sterility (Sotola *et al.*, 2023), its multiple phenotypic effects may reflect *PIL6&7.2*, additional linked genes, and pleiotropic effects of sterility per se (Fishman et al. 2015).

Fig. 5. A flower size NIL. (a) Flowers of the *M. parishii* and *CLL6&7.2* NIL. Scale bar, 4mm. (b) Graphical genotype of the *CLL6&7.2* NIL. The colored bars represent the 8 chromosomes. Violet indicates regions homozygous for *M. parishii*, while pink indicates heterozygous regions, and blue represents regions homozygous for *M. cardinalis*.

Discussion

We used QTL mapping in three hybrid growouts, as well as NIL construction, to investigate the genetic architecture of pollination syndrome divergence between hummingbird-pollinated *Mimulus cardinalis* and self-pollinated *M. parishii*. Despite post-mating barriers (Sotola *et al.* 2023), these taxa are good models for understanding the early stages of speciation: hybrids between *M. parishii* and *M. cardinalis* are florally diverse (Fig. 1), more fit than their respective hybrids with bee-pollinated *M. lewisii* (Fishman *et al.*, 2013, 2015; Stathos & Fishman, 2014), and a source of ongoing introgression in areas of range overlap (Nelson *et al.*, 2021b). Along with chromosome-scale assemblies for all three taxa and new molecular tools, they provide a foundation to understand the molecular genetic basis, evolutionary history, and speciation consequences of complex pollination syndromes. Below, we first interpret patterns of genetic architecture (the size, number, directionality of QTLs) for pigment and pollinator reward/handling traits, as case studies for connecting QTLs to genes. We then explore how multi-trait dimensional QTLs contribute to the maintenance of floral integration across extremely diverse hybrids

324 (Fig 1). Finally, we discuss insights from transferring a NIL dissection approach from pigment traits to
325 more polygenic dimensional traits.

326 **Genetics of extreme floral divergence – pigment and pollinator reward/handling traits**

327 As expected from previous work in *Erythranthe* monkeyflowers and other systems, the carotenoid (PLC)
328 and anthocyanin (PLA, NGA) pigment traits were oligogenic (Fig. 3; Table S1). Each had a leading major
329 QTL ($r^2 > 0.19$) in the core UC_F_2 population, and two of these (PLC4.1 and NGA4.1) co-occur with the
330 secondary PLA4.1 ($r^2 = 0.14$). Although QTL co-localization among different floral traits has often been
331 interpreted as evidence of pleiotropy, this pigment QTL hotspot illustrates the challenges of dissecting
332 linked QTLs down to distinct molecular elements. The *PLC4.1* QTL and *PLA4.1* QTL are caused by
333 variation in the small RNA locus *YELLOW UPPER* (*YUP*) and the *R2R3-MYB* gene *PETAL LOBE*
334 *ANTHOCYANIN* (*PELAN*), respectively. *YUP* and *PELAN* are separated by a single gene known as
335 *SISTER OF LIGHT AREAS1* (*SOLAR*), which is also a regulator of anthocyanin pigmentation (Liang *et al.*,
336 2022, 2023), and together they form a pigment supergene novel to *Mimulus* section *Erythranthe* (Liang
337 *et al.*, 2023). While it is unknown whether SOLAR, PELAN or another linked gene underlies the
338 coincident nectar guide anthocyanin QTL (*NGA4.1*), QTL co-localization here is clearly due to remarkably
339 tight linkage of multiple pigment genes instead of pleiotropic effects of a single gene.

340 In addition to re-capturing known major genes, however, our multi-trait, multi-population QTL approach
341 also reveals a more complex genetic architecture for pigment traits. We identified four additional QTLs
342 each for petal carotenoids (PLC) and anthocyanins (PLA) and nectar guide anthocyanins (NGA), with
343 widely ranging effects (Table S1). NGA3/PLA3 contains *RED TONGUE* (*RTO*), an R3-MYB gene known to
344 repress anthocyanin biosynthesis in both petal lobes and nectar guides of *M. lewisii* flowers (Ding *et al.*,
345 2020). No QTL includes ROSE INTENSITY (ROI; (Yuan *et al.*, 2013b) which controls the reduced
346 anthocyanin of pale pink Sierran *M. lewisii* relative to *M. cardinalis*. However, PLA6&7, a rare wrong-way
347 QTL at which *M. parishii* alleles confer darker anthocyanin pigmentation, contains several R3-MYBs
348 related to ROI and RTO. Thus, there are many ways to generate and modulate complex floral pigment
349 patterns in *Mimulus* flowers, paralleling the pigment supergenes (Hermann *et al.*, 2013) and layers of
350 complexity (Berardi *et al.*, 2021) of similar pollination syndrome shifts in *Petunia*. Overall, our pigment
351 QTL data provide an unusually nuanced picture of the divergence of floral attraction traits, a roadmap
352 for molecular characterization of the underlying genes, and the opportunity to study their effects on
353 pollination ecology in natural and artificial hybrids.

354 The pollinator reward and handling traits (nectar volume, stigma closure speed, nectar guide trichomes)
355 each are also essentially lost in selfer *M. parishii*. High nectar volume (NEV) maintains high hummingbird
356 visitation rates to *M. cardinalis* (Schemske & Bradshaw, 1999), while touch-sensitive stigma closure (SCS)
357 enhances pollen export in outcrossers (Fetscher, 2001) and degenerates in selfers (Friedman *et al.*,
358 2017). *Mimulus* nectar guide trichomes (NGT) likely facilitate efficient flower-handling by bees, like the
359 snapdragon conical cells with which they share a developmental pathway (Glover *et al.*, 1998). Thus,
360 NEV and SCS may be actively maintained at high values in *M. cardinalis*, while NGT may be under
361 relaxed selection in both *M. cardinalis* and *M. parishii* relative to bee-pollinated *M. lewisii* (Chen & Yuan,
362 2024) and the common ancestor of these taxa. For each, in addition to assessing their individual
363 architectures, we can assess developmental integration with other components of the floral selfing
364 syndrome (Sicard & Lenhard, 2011; Liao *et al.*, 2021) and compare with parallel transitions in other
365 systems.

366 Two QTLs of moderate effect (SCS5 and SCS6&7) contribute to stigma closure variation in the UM_F_2
367 population, but together explain only ~1/3 of the parental difference. In contrast, five QTLs fully
368 explained a similar shift between selfer/noncloser *Mimulus nasutus* and fast-closer *M. guttatus* (Fishman
369 *et al.*, 2024). SCS5, which is in a highly recombining region at the end of Chr5 (<900kb, ~115 genes) is
370 ideal for further genetic dissection of mechanosensitive stigma movement. SCS6&7 which spans ~3.5
371 Mb of *M. cardinalis-M. parishii* Chr6, will be more difficult to fine-map, but contains a Mechanosensitive
372 Channel of Small Conductance-like 10 (MSL10) gene homologous to a highly stigma-expressed
373 mechanosensor in the *M. guttatus* complex (Fishman *et al.*, 2024). Stigma closure QTLs appear
374 independent of other floral traits (Fig. 3), and neither SCS QTL identified here is in a region syntenic to
375 *M. nasutus* x *M. guttatus* QTLs, suggesting abundant genomic targets for independent losses of this
376 complex and novel trait.

377 Nectar volume, with six small-to-moderate sized QTLs in the UC_F_2s and RILs together, has a genetic
378 architecture suggesting even greater complexity, including polygenicity, epistasis, pleiotropy, and gene
379 x environment interactions. This contrasts with the simple genetic architecture invoked for this trait in *M.*
380 *lewisii* x *M. cardinalis* hybrids, which identified a leading QTL explaining 30-50% of the F_2 variance
381 (Bradshaw *et al.*, 1998). Our largest F_2 QTLs, NEV2 and NEV6&7, were much smaller (r^2 = 0.12- 0.17) and
382 all four QTL effects sum to only ~35% of the 46μL parental difference. Moreover, a model including all 2-
383 way QTL interactions found significant ($P < 0.005$) interactions of NEV6&7 with NEV4 and NEV2; along

384 with the strong skew of NEV phenotypes (Fig. S1), this suggests that epistatic interactions may
385 contribute to parental divergence. Nectar volume was correlated with length measures (Fig. 2) and both
386 major NEV QTLs in F_2s are coincident with multi-trait size QTLs (see below). This result intriguingly
387 contrasts with a recent study of floral integration in *Ipomaea* (Liao *et al.*, 2021), where nectar traits
388 formed an evolutionary module only weakly correlated with flower size and few QTL positions were
389 shared. The degree of genetic integration may depend on the specifics of floral development. Some
390 components of nectar volume variation (e.g., post-development sugar or water provisioning) may be
391 independent of flower size genes, whereas others (e.g., nectary size) may be directly downstream of
392 developmental shifts causing reduced flowers in *M. parishii*. Nectar volume was also context-dependent,
393 with no overlap between the UC_F_2 and RIL QTLs. The RIL QTLs NEV5 and NEV8 were both much larger
394 (10.9-14.3 μLs each) than any in UC_F_2s. Differences between greenhouse conditions, as well as major
395 non-Mendelian shifts in allele frequency between the populations (Sotola *et al.*, 2023) may contribute to
396 this mismatch.

397 Mapping of nectar guide trichomes (NGT) revealed similar increases in complexity and novel genomic
398 factors over previous work, even within the single UC_F_2 population. Large differences in nectar guide
399 trichome length between *M. parishii* and *M. lewisii* were recently mapped to a major-effect MIXTA-like
400 MYB transcription factor GUIDELESS (1.13 Mb on CE10 Chr6 (Chen & Yuan, 2024), which was also
401 identified as a key determinant of nectar guide formation (both pigment and cell shape) in *M. lewisii* via
402 mutagenesis (Yuan *et al.*, 2013a). Here, none of the four NGT QTLs includes GUIDELESS, suggesting
403 both a much more complex genetic basis in this wide cross and possibly epistatic interactions masking
404 the effects of nonsynonymous mutations previously inferred to be causal of NGT loss in *M. parishii*
405 relative to bee-pollinated *M. lewisii* (Chen & Yuan, 2024). Overall, even for the nectar trait with a
406 relatively simple genetic architecture in classic studies of pollinator adaptation (Hiesey *et al.*, 1971;
407 Bradshaw *et al.*, 1995, 1998; Schemske & Bradshaw, 1999; Bradshaw & Schemske, 2003), stretching the
408 F_2 variation in this phenotypically wider cross reveals greater genetic complexity and many additional
409 candidate loci for functional and ecological genomic investigations.

410 **Genetic architecture of extreme floral divergence – coordination of dimensional traits**

411 Although floral whorls can evolve on highly divergent paths to produce the remarkable diversity of floral
412 forms across all angiosperms, developmental co-ordination facilitates correlated evolution of floral
413 dimensions within lineages. Standing variation that affects one floral dimension may often have

414 pleiotropic effects on others, allowing for rapid evolutionary divergence along a multi-trait "genetic line
415 of least resistance" (Lande & Arnold, 1983; Schluter, 1996). From this perspective, genetic variants that
416 affect multiple traits have outsized evolutionary influence relative to their single-trait effects, accelerating
417 evolution when selection is parallel but potentially generating tradeoffs when it is not. On the other
418 hand, the key evolutionary steps in pollination syndrome shifts may often require breaking the genetic
419 correlations among dimensional traits within populations, and thus involve rare or novel variation. Both
420 the exertion of sexual parts beyond the corolla in hummingbird pollination and loss of stigma-anther
421 distance in autogamous selfers entail changes in the *relative* lengths of different floral whorls. Similarly,
422 the evolution of hummingbird pollination in tubular flowers often entails shifts in corolla allometry (length
423 vs. width) and, as in *M. cardinalis*, the length vs. width of the corolla limb (Fig. 1). Thus, although many
424 loci may influence overall flower size differences accompanying the evolution of pollination syndromes,
425 key evolutionary shifts in the relative size and position of floral organs must be achieved via specific loci
426 with isolated effects on single traits or via disproportionate shifts in size at many loci.

427 In *M. parishii* x *M. cardinalis* hybrids, we capture both major changes in flower size and more subtle, but
428 important, shifts in shape and stigma-anther separation important for mating system shifts. Strong
429 genetic correlations (Fig. 2) and abundant coincidence of QTLs for different dimensional traits (Fig. 3),
430 while not necessarily due to pleiotropy at every underlying locus, is consistent with a general "flower
431 size" developmental module (Krizek & Anderson, 2013) coordinating both corolla elongation associated
432 with hummingbird pollination and reductions associated with selfing. Co-ordination of dimensions by
433 many QTLs with pleiotropic effects is consistent both with studies of parallel interspecific transitions
434 (Fishman *et al.*, 2002; Goodwillie *et al.*, 2006; Kostyun *et al.*, 2019; Liao *et al.*, 2021) and with a highly
435 pleiotropic and polygenic basis to standing variation for corolla size traits within *M. guttatus* (Troth *et al.*,
436 2018). However, we also identified QTLs with disproportionate effects on different whorls and this subset
437 may be particularly important for divergence in pollination syndromes. For example, the *M. parishii*
438 corolla tube and pistil are the same length, with stamens that are slightly exerted past both (Table 1, Fig.
439 1), whereas the *M. cardinalis* style extends 13mm past the corolla tube and 3mm past the stamens. This
440 dramatic exertion of the style implies the action of several PIL-only loci or many multi-trait size loci with
441 slightly greater effects on pistil length (PIL) than stamen (STL) or corolla tube length (CTL). In the QTL
442 data, we see all possible combinations, including joint PIL/STL length QTLs without effects on SAS (e.g.
443 PIL8.1/STL8.1 in UC_F2), regions affecting all three traits (e.g. STL4.1/PIL4.1/SAS4.1 in UM_F_2), and

444 QTLs that only affect stigma-anther separation (e.g. SAS3.1). The former are candidate for overall flower
445 size while the latter are promising targets for dissecting the genetics of mating system evolution.

446 Dissecting the genes underlying polygenic flower size variation in hybrids

447 To understand the molecular mechanisms of floral evolution and trace the history of such loci across
448 species divergence, we must get our hands on the causal variants. However, while even loci with small
449 effects can be mapped to the nucleotide-level in highly recombining wild populations (Troth *et al.*, 2018;
450 Wessinger *et al.*, 2023), the largest F_2 or RIL QTLs for highly polygenic traits in interspecific hybrids may
451 simply fall in regions of high gene density. Here, as a starting point for genetically dissecting the
452 abundant dimensional loci in these hybrids, we independently used nearly isogenic lines (NILs) to isolate
453 QTLs for pistil length and corolla limb length, which capture flower size variation important for mating
454 system and pollinator divergence. NIL generation with phenotypic selection is a common tool for fine-
455 mapping of focal mutants in *Arabidopsis*, and has been used in *Mimulus* to dissect major loci controlling
456 pigment divergence (Yuan *et al.*, 2013b, 2016; Liang *et al.*, 2022, 2023) and hybrid infertility (Sweigart *et*
457 *al.*, 2006; Barr & Fishman, 2010). In conjunction with QTL mapping, it can provide crucial validation and
458 refinement of coincident QTLs and a path toward molecular characterization.

459 Pistil length often determines the key mating system trait of stigma-anther separation, but its molecular
460 basis in natural populations remains poorly understood. Although chemically induced mutations and
461 inhibition of polar auxin transport can alter pistil length dramatically and independently of other floral
462 dimensions in *Mimulus* (Ding *et al.*, 2021), natural species differences appear highly polygenic and
463 potentially pleiotropic (Tables S1-S2). Our pistil length NIL captured two of the largest PIL QTLs, *PIL4.1*
464 and *PIL6&7.2*. These explain only ~9% (3 mm) and ~3% (1 mm) of the 34mm parental difference in pistil
465 length, respectively, but robustly paralleled the corresponding F_2 QTLs in their effects and additivity
466 across loci. The NIL intervals (4 Mb for PIL4.1; 9Mb for PIL6&7) do not yet have sufficient resolution to
467 distinguish between pleiotropy and linkage disequilibrium for joint effects; the PIL4.1 NIL segregates for
468 stamen and corolla tube length as well as pistil length, also consistent with co-incidence of STL, CTL, PIL
469 and SAS QTL peaks around 3Mb on Chrom4 in the UM_F_2. However, given high recombination on
470 chromosome ends in these hybrids (Liang *et al.* 2022; 2023; Sotola *et al.* 2023), we expect that further
471 dissection of these QTLs by fine-scale recombination mapping will allow us to identify the causal gene(s)
472 affecting all four traits.

473 Mutations in many genes can affect petal size by altering cell size and/or the timing of cell growth that
474 result in changes in cell number and organ size/shape (Sicard *et al.*, 2011; Krizek & Anderson, 2013). In
475 *Mimulus*, the corolla developmental trajectory of small-flowered *M. parishii* is truncated but parallel to
476 similar-shaped but bigger *M. lewisii* (Gurung *et al.*, 2021), while hummingbird-pollinated *M. verbenaceus*
477 develops more slowly over twice as long as *M. parishii*, leading to *M. cardinalis*-like flowers (Chen *et al.*,
478 2022). Similar ontogenetic shifts likely account for the strong genetic correlations and QTL co-incidence
479 of floral size metrics in our *M. parishii* x *M. cardinalis* hybrids, making genes that affect developmental
480 timing the strongest functional candidates within flower size QTLs and NILs. Unfortunately, our flower
481 size NIL CLL6&7, which increases the length of corolla limb, corolla tube, stamen, and pistil, corresponds
482 to a reciprocal translocation (Fishman *et al.*, 2013; Stathos & Fishman, 2014; Sotola *et al.*, 2023). Even
483 with the additional generations of crossing in RILs, this region remains associated with severe hybrid
484 sterility and is resistant to genetic dissection. Thus, complementary approaches will be necessary to
485 narrow down functional candidates within this region. Across all QTLs and traits, additional targeted fine-
486 mapping and analyses of gene expression networks conducted on segregating NILs with distinct
487 phenotypes (Langfelder & Horvath, 2008), promises a detailed understanding of the many contributors
488 to floral trait divergence in monkeyflowers.

489 ***Conclusions –*** Overall, our mapping approaches (F2s, RILs, and NILs) are complementary, with the two
490 F_2 populations providing an overview of floral QTLs and derived isogenic lines providing confirmation
491 and refinement. This multi-pronged approach allowed the description of a polygenic genetic
492 architecture even for pollinator attraction (pigment) and reward traits with major leading QTLs, as well as
493 hotspots for dimensional traits controlled by many QTLs of individually small effects. Independent NIL
494 confirmation of two small pistil length QTLs too weak to detect in every population bolster this
495 inference. These complementary approaches lay a strong foundation for both further molecular genetic
496 characterization and investigations of the evolutionary genomics of species barriers in this classic model
497 system.

498

Acknowledgements

We are grateful to T. Nelson and K. Baesen for assistance with the genotyping and phenotyping at the University of Montana (UM) and to logistical support from the UM ECOR Plant Growth Facility and Genomics Core. We thank C. Liu, M. Opel, and M. Moriarty for plant care in the UConn Botanical Conservatory. We are thankful to S. McCann and P. Beardsley for help in generating the RILs. This work was supported by NSF grants DEB-0846089, DEB-1457763 and OIA-1736249 (to LF), IOS-1827645 (to ALS and YWY), DEB-1350935 (to ALS), and IOS-2319721 (to YWY).

Competing interests

The authors declare no competing interests.

Author contributions

HC – data collection, analysis, and visualization, drafting of manuscript; CSB – data collection, analysis, and visualization; MS – data collection; VAS – data collection, analysis, and visualization, drafting of initial manuscript; ALS – conceptualization, data collection and interpretation, editing of manuscript; YWY – conceptualization, data collection and interpretation, drafting and editing of manuscript; LF – conceptualization, data collection, analysis, visualization and interpretation, drafting and editing of manuscript. All authors read and are accountable for the submitted manuscript.

Data availability

The raw sequence data (PRJNA1003462, PRJNA948041) and individual genotypes (doi:10.5061/dryad.v6wwpzh1m) used for generating linkage maps are publicly available. The phenotype matrices used for quantitative genetics and QTL mapping are archived at Dryad https://datadryad.org/stash/share/lDhHN-mqGkS5zdMy9QIcCWuhDNzqm1npxaDtyjAhO6k and will be fully released upon publication. The raw sequencing data used to identify the potential DNA fragments responsible for the long pistils of the PIL NIL and the large flowers of the CLL NIL have been deposited to NCBI under the accession numbers PRJNA1116746 and PRJNA1117077, respectively, and will be released upon publication.

527 REFERENCES

528

529 **Angert AL. 2009**. The niche, limits to species' distributions, and spatiotemporal variation in demography
530 across the elevation ranges of two monkeyflowers. *Proceedings of the National Academy of Sciences of*
531 *the United States of America* **106**: 19693–19698.

532 **Angert AL, Schemske DW. 2005**. The evolution of species' distributions: reciprocal transplants across
533 the elevation ranges of *Mimulus cardinalis* and *M. lewisii*. *Evolution* **59**: 1671–1684.

534 **Barr CM, Fishman L. 2010**. The nuclear component of a cytonuclear hybrid incompatibility in *Mimulus*
535 maps to a cluster of pentatricopeptide repeat genes. *Genetics* **184**: 455–465.

536 **Barrett SCH. 2002**. The evolution of plant sexual diversity. *Nature Reviews Genetics* **3**: 274–284.

537 **Berardi AE, Esfeld K, Jäggi L, Mandel T, Cannarozzi GM, Kuhlemeier C. 2021**. Complex evolution of
538 novel red floral color in *Petunia*. *The Plant Cell* **33**: 2273–2295.

539 **Bleiweiss R. 2001**. Mimicry on the QT(L): genetics of speciation in *Mimulus*. *Evolution* **55**: 1706–1709.

540 **Bradshaw HD, Otto KG, Frewen BE, McKay JK, Schemske DW. 1998**. Quantitative Trait Loci Affecting
541 Differences in Floral Morphology Between Two Species of Monkeyflower (*Mimulus*). *Genetics* **149**: 367–
542 382.

543 **Bradshaw HD, Schemske DW. 2003**. Allele substitution at a flower colour locus produces a pollinator
544 shift in monkeyflowers. *Nature* **426**: 176–178.

545 **Bradshaw HD, Wilbert SM, Otto KG, Schemske DW. 1995**. Genetic mapping of floral traits associated
546 with reproductive isolation in monkeyflowers (*Mimulus*). *Nature* **376**: 762–765.

547 **Byers KJRP, Vela JP, Peng F, Riffell JA, Bradshaw HD. 2014**. Floral volatile alleles can contribute to
548 pollinator-mediated reproductive isolation in monkeyflowers (Mimulus). *The Plant Journal* **80**: 1031–
549 1042.

550 **Chen H, Xiao Z, Ding B, Diggle PK, Yuan Y-W. 2022**. Modular regulation of floral traits by a PRE1
551 homolog in *Mimulus verbenaceus*: implications for the role of pleiotropy in floral integration. *Horticulture*
552 *Research* **9**: uhac168.

553 **Chen H, Yuan Y-W. 2024**. Genetic basis of nectar guide trichome variation between bumblebee- and
554 self-pollinated monkeyflowers (*Mimulus*): role of the MIXTA-like gene GUIDELESS. *BMC Plant Biology*
555 **24**: 62.

556 **Dellinger AS. 2020**. Pollination syndromes in the 21st century: where do we stand and where may we
557 go? *New Phytologist* **228**: 1193–1213.

558 **Ding B, Li J, Gurung V, Lin Q, Sun X, Yuan Y. 2021**. The leaf polarity factors SGS3 and YABBYs regulate
559 style elongation through auxin signaling in *Mimulus lewisii*. *New Phytologist* **232**: 2191–2206.

560 **Ding B, Patterson EL, Holalu SV, Li J, Johnson GA, Stanley LE, Greenlee AB, Peng F, Bradshaw HD,**
561 **Blinov ML, *et al*. 2020**. Two MYB Proteins in a Self-Organizing Activator-Inhibitor System Produce
562 Spotted Pigmentation Patterns. *Current Biology* **30**: 802–814.

563 **Edwards MB, Choi GPT, Derieg NJ, Min Y, Diana AC, Hodges SA, Mahadevan L, Kramer EM,**
564 **Ballerini ES. 2021**. Genetic architecture of floral traits in bee- and hummingbird-pollinated sister species
565 of *Aquilegia* (columbine). *Evolution* **75**: 2197–2216.

566 **Fenster CB, Armbruster WS, Wilson P, Dudash MR, Thomson JD. 2004**. Pollination syndromes and
567 floral specialization. *Annual Review of Ecology, Evolution, and Systematics* **35**: 375–403.

568 **Fetscher AE. 2001**. Resolution of male-female conflict in an hermaphroditic flower. *Proceedings of the*
569 *Royal Society of London. Series B: Biological Sciences* **268**: 525–529.

570 **Fishman L, Beardsley P, Stathos A, Williams CF, Hill JP. 2015**. The genetic architecture of traits
571 associated with the evolution of self-pollination in *Mimulus*. *New Phytologist* **205**: 907–917.

572 **Fishman L, Kelly AJ, Willis JH. 2002**. Minor quantitative trait loci underlie floral traits associated with
573 mating system divergence in *Mimulus*. *Evolution* **56**: 2138–2155.

574 **Fishman L, McIntosh M, Nelson TC, Baesen K, Finseth FR, Stark-dykema E. 2024**. Undoing the 'nasty:
575 dissecting touch-sensitive stigma movement (thigmonasty) and its loss in self-pollinating monkeyflowers.
576 *Biorxiv*.

577 **Fishman L, Stathos A, Beardsley P, Williams CF, Hill JP. 2013**. Chromosomal rearrangements and the
578 genetics of reproductive barriers in Mimulus (monkeyflowers). *Evolution* **67**: 2547–2560.

579 **Friedman J, Hart KS, Bakker MC den. 2017**. Losing one's touch: Evolution of the touch-sensitive stigma
580 in the Mimulus guttatus species complex. *American Journal of Botany* **104**: 335–341.

581 **Glover BJ, Perez-Rodriguez M, Martin C. 1998**. Development of several epidermal cell types can be
582 specified by the same MYB-related plant transcription factor. *Development* **125**: 3497–3508.

583 **Goodwillie C, Kalisz S, Eckert CG. 2005**. The evolutionary enigma of mixed mating systems in plants:
584 occurrence, theoretical explanations, and empirical evidence. *Annual Review of Ecology, Evolution, and*
585 *Systematics* **36**: 47–79.

586 **Goodwillie C, Ritland C, Ritland K. 2006**. The genetic basis of floral traits associated with mating system
587 evolution in Leptosiphon (Polemoniaceae): an analysis of quantitative trait loci. *Evolution* **60**: 491–504.

588 **Gurung V, Yuan Y-W, Diggle PK. 2021**. Comparative analysis of corolla tube development across three
589 closely related Mimulus species with different pollination syndromes. *Evolution & Development* **23**: 244–
590 255.

591 **Hermann K, Klahre U, Moser M, Sheehan H, Mandel T, Kuhlemeier C. 2013**. Tight genetic linkage of
592 prezygotic barrier loci creates a multifunctional speciation island in Petunia. *Current Biology* **23**: 873–
593 877.

594 **Hiesey W, Nobs M, Bjorkman O. 1971**. *Experimental studies on the nature of species: 5.*
595 *Biosystematics, genetics and physiological ecology of the Erythranthe section of Mimulus*. Carnegie
596 Institution.

597 **Klahre U, Gurba A, Hermann K, Saxenhofer M, Bossolini E, Guerin PM, Kuhlemeier C. 2011**. Pollinator
598 choice in Petunia depends on two major genetic Loci for floral scent production. *Current Biology* **21**:
599 730–739.

600 **Kostyun JL, Gibson MJS, King CM, Moyle LC. 2019**. A simple genetic architecture and low constraint
601 allow rapid floral evolution in a diverse and recently radiating plant genus. *New Phytologist* **223**: 1009–
602 1022.

603 **Krizek BA, Anderson JT. 2013**. Control of flower size. *Journal of Experimental Botany* **64**: 1427–1437.

604 **Lande R, Arnold SJ. 1983**. The measurement of selection on correlated characters. *Evolution* **37**: 1210–
605 1226.

606 **Langfelder P, Horvath S. 2008**. WGCNA: an R package for weighted correlation network analysis. *BMC*
607 *Bioinformatics* **9**: 559.

608 **Liang M, Chen W, LaFountain AM, Liu Y, Peng F, Xia R, Bradshaw HD, Yuan Y-W. 2023**. Taxon-
609 specific, phased siRNAs underlie a speciation locus in monkeyflowers. *Science* **379**: 576–582.

610 **Liang M, Foster CE, Yuan Y-W. 2022**. Lost in translation: Molecular basis of reduced flower coloration in
611 a self-pollinated monkeyflower (*Mimulus*) species. *Science Advances* **8**: eabo1113.

612 **Liao IT, Rifkin JL, Cao G, Rausher MD. 2021**. Modularity and selection of nectar traits in the evolution of
613 the selfing syndrome in *Ipomoea lacunosa* (Convolvulaceae). *New Phytologist* **233**: 1505–1519.

614 **Lowry DB, Willis JH. 2010**. A widespread chromosomal inversion polymorphism contributes to a major
615 life-history transition, local adaptation, and reproductive isolation. *PLoS Biology* **8**: e1000500.

616 **Nelson TC, Muir CD, Stathos AM, Vanderpool DD, Anderson K, Angert AL, Fishman L. 2021a**.
617 Quantitative trait locus mapping reveals an independent genetic basis for joint divergence in leaf
618 function, life-history, and floral traits between scarlet monkeyflower (*Mimulus cardinalis*) populations.
619 *American Journal of Botany* **108**: 844–856.

620 **Nelson TC, Stathos AM, Vanderpool DD, Finseth FR, Yuan Y-W, Fishman L. 2021b**. Ancient and recent
621 introgression shape the evolutionary history of pollinator adaptation and speciation in a model
622 monkeyflower radiation (*Mimulus* section *Erythranthe*). *PLoS Genetics* **17**: e1009095.

623 **Orr HA. 1998**. Testing natural selection vs. genetic drift in phenotypic evolution using quantitative trait
624 locus data. *Genetics* **149**: 2099–2104.

625 **Peng F, Byers KJRP, Bradshaw HD. 2017**. Less is more: Independent loss-of-function OCIMENE
626 SYNTHASE alleles parallel pollination syndrome diversification in monkeyflowers (*Mimulus*). *American*
627 *Journal of Botany* **104**: 1055–1059.

628 **Ramsey J, Bradshaw HD, Schemske DW. 2003**. Components of reproductive isolation between the
629 monkeyflowers Mimulus lewisii and M. cardinalis (Phrymaceae). *Evolution* **57**: 1520–1534.

630 **Rifkin JL, Cao G, Rausher MD. 2021**. Genetic architecture of divergence: the selfing syndrome in
631 Ipomoea lacunosa. *American Journal of Botany* **108**: 2038–2054.

632 **Schemske DW, Bradshaw HD. 1999**. Pollinator preference and the evolution of floral traits in
633 monkeyflowers (Mimulus). *Proceedings of the National Academy of Sciences of the United States of*
634 *America* **96**: 11910–11915.

635 **Schluter D. 1996**. Adaptive radiation along genetic lines of least resistance. *Evolution* **50**: 1766–1774.

636 **Sicard A, Lenhard M. 2011**. The selfing syndrome: a model for studying the genetic and evolutionary
637 basis of morphological adaptation in plants. *Annals of Botany* **107**: 1433–1443.

638 **Sicard A, Stacey N, Hermann K, Dessoly J, Neuffer B, Bäurle I, Lenhard M. 2011**. Genetics, evolution,
639 and adaptive significance of the selfing syndrome in the genus Capsella. *The Plant Cell* **23**: 3156–3171.

640 **Smith SD. 2016**. Pleiotropy and the evolution of floral integration. *New Phytologist* **209**: 80–85.

641 **Sotola VA, Berg CS, Samuli M, Chen H, Mantel SJ, Beardsley PA, Yuan Y-W, Sweigart AL, Fishman L.**
642 **2023**. Genomic mechanisms and consequences of diverse postzygotic barriers between monkeyflower
643 species. *Genetics* **225**: iyad156.

644 **Stankowski S, Chase MA, McIntosh H, Streisfeld MA. 2023**. Integrating top-down and bottom-up
645 approaches to understand the genetic architecture of speciation across a monkeyflower hybrid zone.
646 *Molecular Ecology* **32**: 2041–2054.

647 **Stathos A, Fishman L. 2014**. Chromosomal rearrangements directly cause underdominant F_1 pollen
648 sterility in *Mimulus lewisii–Mimulus cardinalis* hybrids. *Evolution* **68**: 3109–3119.

649 **Stebbins GL. 1970**. Adaptive radiation of reproductive characteristics in angiosperms I: Pollination
650 mechanisms. *Annual Review of Ecology and Systematics* **1**: 307–326.

651 **Stuurman J, Hoballah ME, Broger L, Moore J, Basten C, Kuhlemeier C. 2004**. Dissection of Floral
652 Pollination Syndromes in Petunia. *Genetics* **168**: 1585–1599.

653 **Sweigart AL, Fishman L, Willis JH. 2006**. A simple genetic incompatibility causes hybrid male sterility in
654 *Mimulus. Genetics* **172**: 2465–2479.

655 **Troth A, Puzey JR, Kim RS, Willis JH, Kelly JK. 2018**. Selective trade-offs maintain alleles underpinning
656 complex trait variation in plants. *Science* **361**: 475–478.

657 **Wang S, Basten CJ, Zeng Z-B. 2005**. *Windows QTL Cartographer 2.5*. Dept. of Statistics, North Carolina
658 State Univ.

659 **Wessinger CA, Hileman LC. 2016**. Accessibility, constraint, and repetition in adaptive floral evolution.
660 *Developmental Biology* **419**: 175–183.

661 **Wessinger CA, Katzer AM, Hime PM, Rausher MD, Kelly JK, Hileman LC. 2023**. A few essential
662 genetic loci distinguish *Penstemon* species with flowers adapted to pollination by bees or
663 hummingbirds. *PLOS Biology* **21**: e3002294.

664 **Wilson P, Wolfe AD, Armbruster WS, Thomson JD. 2007**. Constrained lability in floral evolution:
665 counting convergent origins of hummingbird pollination in *Penstemon* and *Keckiella*. *New Phytologist*
666 **176**: 883–890.

667 **Yeaman S, Whitlock MC. 2011**. The genetic architecture of adaptation under migration-selection
668 balance. *Evolution* **65**: 1897–1911.

669 **Yuan Y-W. 2019**. Monkeyflowers (*Mimulus*): new model for plant developmental genetics and evo-devo.
670 *New Phytologist* **222**: 694–700.

671 **Yuan Y-W, Rebocho AB, Sagawa JM, Stanley LE, Bradshaw HD. 2016**. Competition between
672 anthocyanin and flavonol biosynthesis produces spatial pattern variation of floral pigments between
673 *Mimulus* species. *Proceedings of the National Academy of Sciences of the United States of America* **113**:
674 2448–2453.

675 **Yuan Y-W, Sagawa JM, Frost L, Vela JP, Bradshaw HD. 2014**. Transcriptional control of floral
676 anthocyanin pigmentation in monkeyflowers (*Mimulus*). *New Phytologist* **204**: 1013–1027.

677 **Yuan Y-W, Sagawa JM, Stilio VSD, Bradshaw HD. 2013a**. Bulk segregant analysis of an induced floral
678 mutant identifies a MIXTA-like R2R3 MYB controlling nectar guide formation in *Mimulus lewisii*. *Genetics*
679 **194**: 523–528.

680 **Yuan Y-W, Sagawa JM, Young RC, Christensen BJ, Bradshaw HD. 2013b**. Genetic dissection of a
681 major anthocyanin QTL contributing to pollinator-mediated reproductive isolation between sister species
682 of *Mimulus*. *Genetics* **194**: 255–263.

683